Monthly Notices
of the
ROYAL ASTRONOMICAL SOCIETY

Mon. Not. R. Astron. Soc. **413,** 132–148 (2011) doi:10.1111/j.1365-2966.2010.18115.x

Statistical properties of polarized radio sources at high frequency and their impact on cosmic microwave background polarization measurements

R. A. Battye,⋆ I. W. A. Browne, M. W. Peel, N. J. Jackson and C. Dickinson

Jodrell Bank Centre for Astrophysics, School of Physics and Astronomy, The University of Manchester, Oxford Road, Manchester M13 9PL

Accepted 2010 November 27. Received 2010 November 24; in original form 2010 March 30

ABSTRACT

We have studied the implications of high-sensitivity polarization measurements of objects from the *Wilkinson Microwave Anisotropy Probe* (*WMAP*) point source catalogue made using the Very Large Array (VLA) at 8.4, 22 and 43 GHz. The fractional polarization of sources is almost independent of frequency with a median of ≈2 per cent and an average, for detected sources, of ≈3.5 per cent. These values are also independent of the total intensity over the narrow range of intensity we sample. Using a contemporaneous sample of 105 sources detected at all three VLA frequencies, we have investigated the spectral behaviour as a function of frequency by means of a two-colour diagram. Most sources have power-law spectra in total intensity, as expected. On the other hand, they appear to be almost randomly distributed in the polarized intensity two-colour diagram. This is compatible with the polarized spectra being much less smooth than those in intensity and we speculate on the physical origins of this. We have performed an analysis of the correlations between the fractional polarization and spectral indices including computation of the principal components. We find that there is little correlation between the fractional polarization and the intensity spectral indices. This is also the case when we include polarization measurements at 1.4 GHz from the NRAO VLA Sky Survey (NVSS). In addition we compute 45 rotation measures from polarization position angles which are compatible with a λ^2 law. We use our results to predict the level of point source confusion noise that contaminates cosmic microwave background polarization measurements aimed at detecting primordial gravitational waves from inflation. We conclude that some level of source subtraction will be necessary to detect $r \sim 0.1$ below 100 GHz and at all frequencies to detect $r \sim 0.01$. We present estimates of the level of contamination expected and the number of sources which need to be subtracted as a function of the imposed cut flux density and frequency.

Key words: polarization – catalogues – galaxies: general – radio continuum: galaxies – cosmic microwave background.

1 INTRODUCTION

Synchrotron radiation is the primary emission mechanism for sources detected in the radio band. Hence, radio sources are likely to be linearly polarized with a fractional polarization of typically a few per cent, depending on the level of the order of the magnetic field in the emission-producing regions. Large-scale polarization catalogues exist for sources selected at low frequencies such as 1.4 GHz (NVSS; Condon et al. 1998) with $\approx 2 \times 10^5$ detections. At higher frequencies, Jackson et al. (2007) have looked at flat spectrum sources in the CLASS survey (Myers et al. 2003; Browne et al. 2003) and have ≈5000 detections of 8.4 GHz polarizations. In recent times more information has become available at even higher frequencies. Ricci et al. (2004) have detected significant polarization in 170 sources at 18.5 GHz, while Massardi et al. (2008) present the results from follow-up of the AT20G survey (Sadler et al. 2006). They have detected polarization at 22 GHz in 218 sources with total intensity greater than 0.5 Jy at 22 GHz with additional information at 4.8 and 8.4 GHz. Murphy et al. (2010) present the full AT20G survey containing 5890 sources stronger than 40 mJy at 20 GHz. Most sources have near-simultaneous 5 and 8 GHz measurements and 1559 have detections of polarized emission at one or more frequencies. In addition, Agudo et al. (2009) have presented measurements of 146 sources at 86 GHz made using the Institut de Radio Astronomie Millimetrique (IRAM)

⋆E-mail: Richard.Battye@manchester.ac.uk

telescope and Lopez-Caniego et al. (2009) have created a catalogue of polarized sources detected from the *Wilkinson Microwave Anisotropy Probe* (*WMAP*) maps between 22 and 90 GHz.

Our main motivation for studying the properties of polarized radio sources is to assess their potential contamination of cosmic microwave background (CMB) polarization data. Measurements have been made of the so-called E-mode polarization which is produced by scalar density fluctuations (Kovac et al. 2002; Readhead et al. 2004; Montroy et al. 2006; Page et al. 2007; Brown et al. 2009; Chiang et al. 2010). Future instruments are aimed at detecting the B-mode signature of primordial gravitational waves produced by inflation (see e.g. Baumann et al. 2009) which is often quantified in terms of the scalar-to-tensor ratio, r. These will require not only high signal-to-noise ratio, but also exquisite control of systematics and separation of astrophysical foregrounds. To date the only work on this issue (de Zotti et al. 1999; Mesa et al. 2002; Tucci et al. 2005) has relied on extrapolation of polarized source counts from frequencies which are factors of $\approx$20 lower than where the CMB observations will take place.

We will focus on the implications of the measurements we have obtained for a sample of 203 radio sources extracted from the *WMAP* 22 GHz catalogue which was complete to $\approx$1 Jy. Most of these sources were also detected in the NVSS (Condon et al. 1998) at 1.4 GHz and 71 were detected at 86 GHz using the IRAM telescope by Agudo et al. (2009); we will make use of this information later. We studied sources in the region with declinations greater than -34° and all were observed at 22 and 43 GHz using the Very Large Array (VLA). A subset of 134 were also observed at 8.4 GHz. Observations were missing for three sources due to misidentifications and a further seven sources were deemed inappropriate to include in the present statistical analysis for a variety of reasons such as the source being very extended and being heavily resolved in our VLA observations. Polarized emission was detected for 123, 169 and 167 sources at 8.4, 22 and 43 GHz, respectively, and 105 were detected at all three frequencies. No polarization bias correction was applied since all detections are greater than 5σ and many are substantially stronger. This 'contemporaneous sample' provides the first direct information at frequencies relevant to CMB measurements allowing more accurate extrapolations to be made. The details of the observations and the catalogue are presented in Jackson et al. (2010).

2 STATISTICAL PROPERTIES OF THE CONTEMPORANEOUS SAMPLE

In this section, we will focus on the sample of 105 sources in which polarized emission was detected at all three frequencies. Since all these measurements were made on a single day they provide a snapshot of the polarized source population and are unlikely to be significantly affected by the variability that can be important for such sources. Although it will be biased in some complicated way towards objects which had strong polarized emission at the time of observation, this sample is particularly useful for investigating the properties of the sources as a function of frequency. In the following section, we will describe our analysis of all our measurements plus those made at 8.4 GHz as part of the CLASS program, at 1.4 GHz from the NVSS and at 86 GHz using the IRAM telescope which were taken at different times and could be affected by variability.

2.1 Summary of basic properties

We define the intensity spectral index, with $S \propto \nu^{\alpha}$ between frequencies ν_1 and ν_2 by $\alpha_{\nu_1}^{\nu_2}$, and the corresponding spectral index

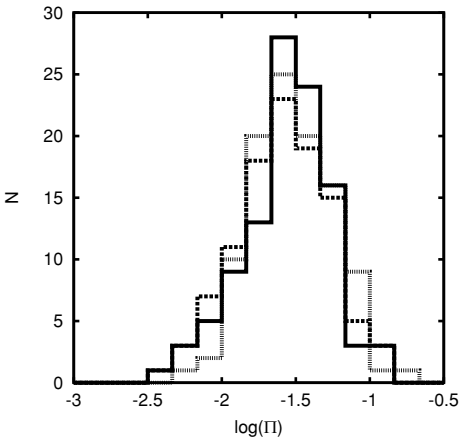

Figure 1. Histogram of the number sources in the contemporaneous sample as a function of the logarithm of the fractional polarization, log (Π). The solid line is for 8.4 GHz, the dashed line is for 22 GHz and the dotted line is for 43 GHz. The distributions of fractional polarizations appear to be relatively independent of frequency. It should be possible to model each of them as a Gaussian in log (Π) with a reasonable degree of accuracy as discussed in Section 5.

for polarized intensity, defined in terms of the Stokes parameters Q and U by $P = \sqrt{Q^2 + U^2}$, as $\beta_{\nu_1}^{\nu_2}$. The fractional polarization at frequency ν is defined to be $\Pi_\nu = P_\nu / S_\nu$. In an analogous way to the total and polarized intensity, one can also define a spectral index for the fractional polarization, $\gamma_{\nu_1}^{\nu_2}$.

Histograms of the fractional polarization are presented in Fig. 1 . It is clear that the distributions only vary very slightly, if at all, as a function of frequency. The mean fractional polarization is computed to be $100\langle\Pi\rangle = 3.3$, 3.3 and 3.7 at 8.4, 22, 43 GHz and the rms is $100\langle\Pi^2\rangle^{1/2} = 3.9$, 4.1 and 4.7. Approximately the same level of fractional polarization was seen in the sample studied by Massardi et al. (2008). The results suggest that fractional polarization is approximately constant as a function of frequency, although there is an increase in the dispersion as frequency increases, something that is also seen in the Massardi et al. (2008) data.

Histograms of the intensity, polarized intensity and fractional polarization spectral indices are presented in Fig. 2. There is a shift in the intensity spectral index distribution as one goes from 8.4–22 GHz to 22–43 GHz indicating, as expected, that on average the intensity spectrum is steepening as one goes to higher frequencies. The polarized intensity spectral index distributions appear to be consistent with no significant variation with frequency. The mean and rms spectral indices within the sample were computed to be $\alpha_{8.4}^{22} = -0.17 \pm 0.36$, $\alpha_{22}^{43} = -0.44 \pm 0.47$, $\beta_{8.4}^{22} = -0.23 \pm 0.85$, $\beta_{22}^{43} = -0.20 \pm 0.81$, $\gamma_{8.4}^{22} = -0.06 \pm 0.84$ and $\gamma_{22}^{43} = 0.24 \pm 0.67$ where the dispersion is quantified by the standard deviation within the sample and is not the error on the mean (which would be smaller by a factor of $1/\sqrt{N}$). Of course the αs, βs and γs are not independent, thus since β is approximately the same for the two frequency ranges and α becomes more negative for the higher frequency range, γ will be more positive in the higher range.

2.2 Two-colour diagrams

In Fig. 3, we present two-colour diagrams for the intensity and polarized emission for the spectral indices between 8.4 and 22 GHz, and between 22 and 43 GHz. These are larger versions of plots presented in Fig. 4. We define the region $|\alpha_{8.4}^{22}| < 0.3$ and $|\alpha_{22}^{43}| < 0.3$ to be flat spectrum in intensity. Excluding this region, the four

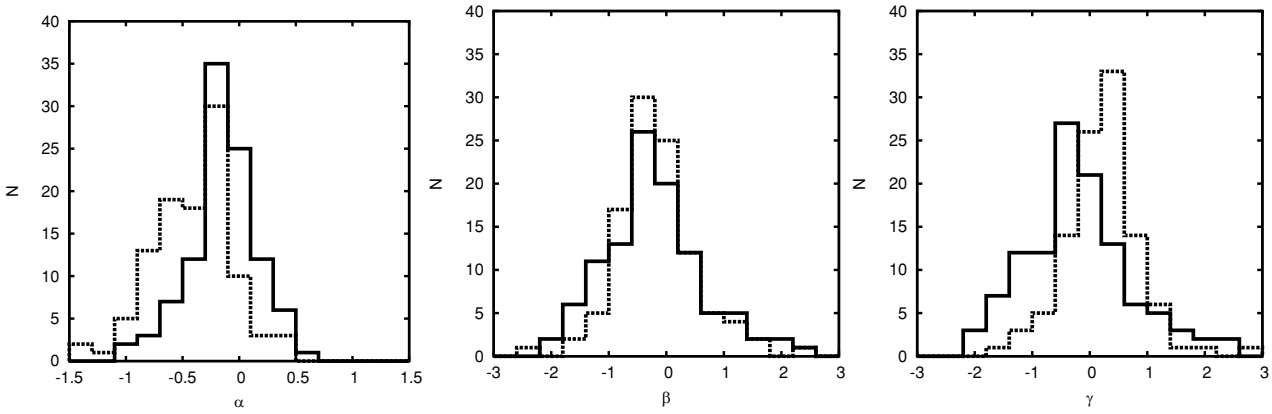

Figure 2. Histograms of the number of sources in the contemporaneous sample as a function of the spectral indices for the intensity (left), polarized intensity (middle) and fractional polarization (right). Solid lines are the spectral indices measured between 8.4 and 22 GHz and the dashed lines between 22 and 43 GHz. The intensity histograms are offset for each other, whereas those for the polarized intensity are very similar over the two different frequency ranges.

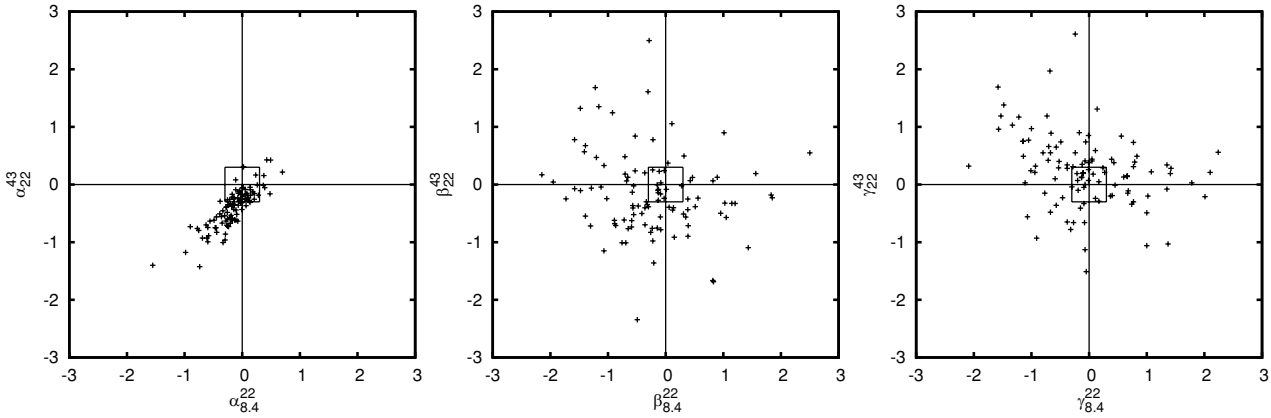

Figure 3. The two-colour diagram (8.4-22-43) for intensity (left), polarized intensity (middle) and fractional polarization (right) for the contemporaneous sample. The upper-left-hand column quadrant corresponds to upturn (U) sources, the upper-right-hand quadrant to inverted (I) sources, the lower-left hand quadrant to steep spectrum (S) sources and the lower-right-hand quadrant to peaked spectrum (P) sources. The box in the middle corresponds to the flat spectrum region (F). There is a strong correlation between $\alpha^{22}_{8.4}$ and α^{43}_{22}, very little correlation between $\beta^{22}_{8.4}$ and β^{43}_{22}, and an anti-correlation between $\gamma^{22}_{8.4}$ and γ^{43}_{22}. There are a number of upturn sources in both polarized intensity and fractional polarization in marked contrast to intensity.

quadrants of the plot correspond to steep spectrum ($\alpha^{22}_{8.4} < 0$ and $\alpha^{43}_{22} < 0$), peaked ($\alpha^{22}_{8.4} > 0$ and $\alpha^{43}_{22} < 0$), inverted ($\alpha^{22}_{8.4} > 0$ and $\alpha^{43}_{22} > 0$) and upturn ($\alpha^{22}_{8.4} < 0$ and $\alpha^{43}_{22} > 0$). We will denote the upturn, inverted, flat, peaked and steep spectrum regions by the letters U, I, F, P and S, respectively. Similar definitions can be made for the spectral indices of the polarized intensity and fractional polarization.

Most of the sources have roughly power-law spectra in total intensity; there are very few peaked sources, a few inverted sources and no sources whose spectra upturn. The numbers of sources in the different categories are (U, I, F, P, S) = (0, 5, 37, 5, 58). There is a strong correlation (correlation coefficient 0.83) between the two intensity spectral indices, and most spectral indices are in the range $-1.5 < \alpha < 0.5$.

The situation is very different for the polarized spectral indices. There appears to be no correlation (correlation coefficient −0.11) between the two polarization spectral indices, with each of the four quadrants in Fig. 3 being populated by significant numbers of sources. The numbers in the different categories are (U, I, F, P, S) = (21, 10, 13, 22, 39). Also worthy of note is the fact that there are a number of sources which have upturn spectra in polarized flux density in this frequency range.

The range of fractional polarization spectral indices is also large, but there is now an anti-correlation (correlation coefficient −0.59) between the indices in the two frequency ranges. The numbers of sources in each of the categories are (U, I, F, P, S) = (39, 21, 18, 13, 14). More sources have increasing fractional polarizations with frequency than decreasing and, if such a trend is continued to frequencies ≈100 GHz, this could have significant implications for CMB observations.

In order to explore the complex interaction between the spectral behaviour in intensity, polarized intensity and fractional polarization we have computed two matrices as done in Massardi et al. (2008). These matrices are presented in Tables 1 and 2. Each of the columns corresponds to a spectral type in intensity and each of the rows the equivalent in either polarized intensity or fractional polarization.

2.3 Correlations between fractional polarization and spectral indices

We can also perform a correlation analysis between the fractional polarization, Π, and the spectral indices α and β. There are many possible correlations which could be presented between three

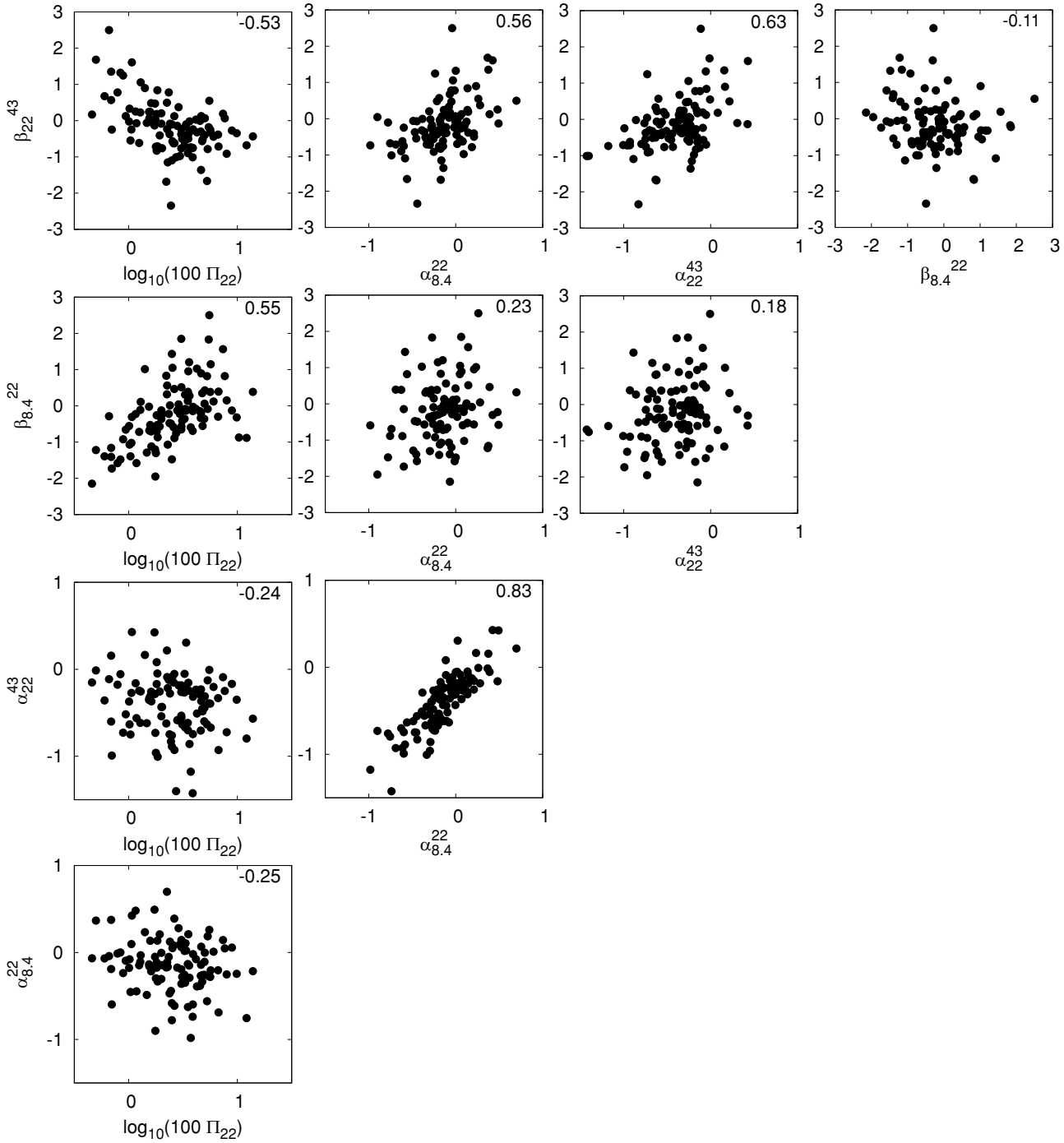

Figure 4. Correlations between five derived quantities, $\log_{10}\Pi_{22}$, $\alpha_{8.4}^{22}$, α_{22}^{43}, $\beta_{8.4}^{22}$ and β_{22}^{43}, for the contemporaneous sample, along with a table of correlation coefficients. The strongest correlation is between $\alpha_{8.4}^{22}$ and α_{22}^{43}.

fractional polarizations and six spectral indices. However, not all are independent. Extracting out the overall intensity flux scale $\approx$1 Jy which is natural when considering ratios (or logs of ratios), we have chosen to present correlations between five quantities, the logarithm of the fractional polarization at 22 GHz, Π_{22}, and the spectral indices, both in intensity and in polarization, to the other two frequencies, $\alpha_{8.4}^{22}, \alpha_{22}^{43}$ and $\beta_{8.4}^{22}, \beta_{22}^{43}$. The results of this are presented in Fig. 4.

We have performed a principal component analysis (PCA) of this combination of data using five variables ($\log_{10}\Pi_{22}$, $\alpha_{8.4}^{22}$, α_{22}^{43}, $\beta_{8.4}^{22}$, β_{22}^{43}). The principal components are

$$
\begin{aligned}
c_1 &= -0.30\log_{10}\Pi_{22} - 0.77\alpha_{8.4}^{22} + 0.55\alpha_{22}^{43} + 0.08\beta_{8.4}^{22} - 0.07\beta_{22}^{43},\\
c_2 &= 0.92\log_{10}\Pi_{22} - 0.22\alpha_{8.4}^{22} + 0.24\alpha_{22}^{43} - 0.19\beta_{8.4}^{22} - 0.15\beta_{22}^{43},\\
c_3 &= -0.01\log_{10}\Pi_{22} - 0.50\alpha_{8.4}^{22} + 0.67\alpha_{22}^{43} + 0.20\beta_{8.4}^{22} - 0.50\beta_{22}^{43},\\
c_4 &= 0.12\log_{10}\Pi_{22} + 0.23\alpha_{8.4}^{22} + 0.29\alpha_{22}^{43} + 0.88\beta_{8.4}^{22} + 0.26\beta_{22}^{43},\\
c_5 &= -0.24\log_{10}\Pi_{22} + 0.21\alpha_{8.4}^{22} + 0.33\alpha_{22}^{43} - 0.37\beta_{8.4}^{22} + 0.81\beta_{22}^{43}.
\end{aligned}
\quad (1)
$$

Table 1. Matrix containing the number of sources with a given spectral type in intensity (columns) and polarized intensity (rows) for the contemporaneous sample. U, I, F, P, S signify the upturn, inverted, flat, peaked and steep spectrum spectral types defined in the text.

	U	I	F	P	S
U	0	2	9	2	8
I	0	1	6	2	1
F	0	1	4	1	7
P	0	0	7	0	15
S	0	1	11	0	27

Table 2. Matrix containing the number of sources with a given spectral type in intensity (columns) and fractional polarization (rows) for the contemporaneous sample. U, I, F, P, S signify the upturn, inverted, flat, peaked and steep spectrum spectral types defined in the text.

	U	I	F	P	S
U	0	3	11	3	22
I	0	0	6	1	14
F	0	0	6	1	11
P	0	0	5	0	8
S	0	2	9	0	3

These are listed in order of ascending variance, that is, the first component has the lowest variance. We find that $c_1 = 0.36 \pm 0.16$, $c_2 = -1.51 \pm 0.21$, $c_3 = -0.22 \pm 0.36$, $c_4 = -0.61 \pm 0.86$ and $c_5 = 0.13 \pm 0.93$. The lowest variance component suggests that there is a complicated connection between the fractional polarized intensity and the total intensity and polarized intensity spectral indices.

This can be further investigated by performing a PCA using just two $(\alpha_{22}^{43}, \alpha_{8.4}^{22})$ and three $(\log_{10}\Pi_{22}, \alpha_{22}^{43}, \alpha_{8.4}^{22})$ variables. We find that the lowest variance components for these two cases are $-0.81\alpha_{8.4}^{22} + 0.58\alpha_{22}^{43} = -0.12 \pm 0.17$ and $-0.02\ \log_{10}\Pi_{22} - 0.81\alpha_{8.4}^{22} + 0.59\alpha_{22}^{43} = -0.08 \pm 0.16$, respectively. It is clear that there is a strong correlation between the intensity spectral indices, and they are almost independent of the fractional polarization. Hence, the connection between the fractional polarization and the spectral indices can only be established once the polarized intensity spectral indices are included.

2.4 Rotation measures

It is clear from fig. 6 of Jackson et al. (2010) and from their table 2 that the polarization position angles measured for many of the sources are not the same at all three frequencies. If the source is simple and there is a simple Faraday screen, then one would expect the measured position angle to satisfy $\phi = \phi_{\rm int} + {\rm RM}\lambda^2$ where $\phi_{\rm int}$ is the intrinsic position angle and RM is the rotation measure. However, many sources are not compatible with this simple law and there are several possible reasons for this:

(i) it could arise from the polarization position angle of a single component changing as it moves from being optically thick to being optically thin;

(ii) the source could have multiple components each having different spectral indices and each with different intrinsic polarization position angles and/or suffering different Faraday rotations;

(iii) it could result from the different resolutions of the observations at the different frequencies being more or less sensitive to different parts of the source having different polarization position angles;

or a combination of these reasons.

We have looked for the λ^2 dependence in all those sources with three contemporaneous detections of polarization. The method we use is to compute the rotation measures necessary to be compatible with each of the two angle differences $\phi_{22} - \phi_{43} = 7.8 \times 10^{-3}\,{\rm deg}({\rm RM/rad\,m^{-2}})$ and $\phi_{8.4} - \phi_{22} = 6.2 \times 10^{-2}\,{\rm deg}({\rm RM/rad\,m^{-2}})$. The errors on the combined rotation measure and the intrinsic position angle are computed by combining errors in quadrature. Those which are compatible within the 2σ errors are deemed to be acceptable. The angle difference $\phi_{8.4} - \phi_{22}$ is more sensitive to rotation than $\phi_{22} - \phi_{43}$ and hence we allow for $\pm 180^\circ$ or $\pm 360^\circ$ to be added to $\phi_{8.4} - \phi_{22}$ in order to account for possible ambiguities inherent in estimating rotation measures for three angle measurements.

We find satisfactory λ^2 fits for 45 of the 105 sources and the resulting rotation measures are presented in Table 3. We caution against believing every individual rotation measure since the process of adding $\pm 180^\circ$ and $\pm 360^\circ$ can lead to some spurious matches to the λ^2 law but the fact that the position angle measurements typically have error bars $< \pm 10^\circ$ will make this unlikely.

We have plotted a histogram of |RM| in Fig. 5. This appears to show strong statistical evidence for a significant number of compact sources which have intrinsic rotation measures in excess of $1000\,{\rm rad\,m^{-2}}$ and at high galactic latitudes such high rotation measures cannot be of Galactic origin. This result is not unexpected since *VLBI* measurements, for example Zavala & Taylor (2003), find evidence of rotation measures of this order in the milliarcsec cores of compact radio sources. In most of our targets the emission is dominated by such compact cores and therefore we might expect comparable rotation measures for the whole source and the compact core alone.

We have compared our results with those available in the literature. There are only four sources common to our list and to the Zavala & Taylor (2003) list. For one they could not get a satisfactory λ^2 fit, for two we both have low rotation measures of the order a few $100\,{\rm rad\,m^{-2}}$ and for the last we have a value of $(587 \pm 14)\,{\rm rad\,m^{-2}}$ and they quote $1433\,{\rm rad\,m^{-2}}$. There is no obvious way to reconcile the two values for this last source with a single rotation measure and we suggest that the source probably has different components suffering different rotation measures. Many of the sources in Table 3 are in the list presented in Taylor et al. (2009) which were computed using the two bands around 1.4 GHz in the NVSS. There is very little correspondence between the two. It is clear that it is difficult to make correspondence between rotation measures computed using observations at different frequencies and resolutions.

Though we think it is probably not astrophysically significant, we note that there is statistical evidence for a bias in our sample towards positive values of the rotation measures with there being 30 positive values and only 15 negative. It is also noticeable that there is a long line of positive rotation measures having right ascensions (RAs) between 13 and 18 h. A relatively small ($\approx +80\,{\rm m^{-2}}$) systematic

Table 3. Estimated rotation measurements and intrinsic position angles for 45 sources which appear compatible with the λ^2 law. Notice that there is a substantial region of positive rotation measure in the RA range 13 to 18 h.

Name	$\phi_{8.4}$	ϕ_{22}	ϕ_{43}	RM/rad m^{-2}	$\phi_{\rm int}$
0029+059	116.0 ± 0.5	129.8 ± 3.9	146.9 ± 2.5	−3116 ± 63	138.2 ± 2.5
0050−068	144.8 ± 0.4	145.2 ± 5.1	127.9 ± 1.1	2887 ± 82	136.0 ± 1.1
0121+118	90.3 ± 0.1	15.8 ± 0.9	8.0 ± 0.3	1199 ± 15	11.3 ± 0.3
0308+040	105.0 ± 0.6	63.3 ± 5.1	115.8 ± 5.2	−5146 ± 83	101.4 ± 5.2
0329−239	157.0 ± 0.5	103.7 ± 4.0	110.3 ± 5.0	−2037 ± 65	104.6 ± 5.0
0340−213	132.3 ± 0.4	38.8 ± 3.8	30.3 ± 2.8	1503 ± 62	34.5 ± 2.8
0405−130	157.9 ± 0.5	169.4 ± 1.0	166.4 ± 2.2	−184 ± 18	165.9 ± 2.2
0423+023	126.0 ± 2.4	123.8 ± 3.9	115.9 ± 5.2	43 ± 74	116.0 ± 5.2
0453−281	123.8 ± 2.4	62.6 ± 4.9	11.5 ± 5.8	6791 ± 88	30.5 ± 5.8
0501−019	109.7 ± 0.9	33.4 ± 6.0	34.1 ± 0.8	1210 ± 98	37.5 ± 0.8
0513−219	122.1 ± 1.7	135.9 ± 4.1	134.1 ± 1.2	−215 ± 72	133.5 ± 1.2
0608−223	89.2 ± 0.4	50.0 ± 2.2	45.3 ± 0.8	632 ± 36	47.0 ± 0.8
0721+713	180.0 ± 0.1	28.5 ± 5.6	52.0 ± 0.3	−3357 ± 90	42.6 ± 0.4
0738+177	147.4 ± 0.8	160.7 ± 2.3	154.7 ± 4.0	−211 ± 40	154.1 ± 4.0
0750+125	69.4 ± 0.4	33.2 ± 0.8	27.1 ± 0.5	588 ± 14	28.7 ± 0.5
0757+099	46.7 ± 0.2	23.0 ± 1.3	17.8 ± 0.8	386 ± 22	18.9 ± 0.8
0813+482	11.9 ± 0.5	134.4 ± 2.2	119.2 ± 3.9	931 ± 36	121.8 ± 3.9
0902−142	84.7 ± 0.2	56.8 ± 4.1	102.1 ± 4.0	−5361 ± 66	87.1 ± 4.0
0914+028	104.6 ± 0.4	119.7 ± 2.5	119.7 ± 2.3	−241 ± 40	119.0 ± 2.3
0920+446	162.6 ± 0.4	126.3 ± 2.0	93.3 ± 2.5	3492 ± 32	103.1 ± 2.5
0958+473	19.5 ± 0.5	150.0 ± 3.0	156.4 ± 4.6	−2099 ± 49	150.5 ± 4.6
1041+061	80.1 ± 0.3	36.3 ± 2.8	34.1 ± 2.6	703 ± 46	36.0 ± 2.6
1130−148	131.6 ± 0.1	167.8 ± 2.8	157.9 ± 4.0	2314 ± 45	164.4 ± 4.0
1153+495	90.6 ± 0.2	14.3 ± 3.3	26.0 ± 4.9	−1671 ± 54	21.3 ± 4.9
1155+810	74.0 ± 0.4	86.0 ± 2.3	73.6 ± 4.6	2705 ± 38	81.1 ± 4.6
1331+305	33.0 ± 0.3	32.7 ± 0.8	32.6 ± 0.4	5 ± 13	32.6 ± 0.4
1354−106	152.7 ± 0.4	35.9 ± 3.7	14.5 ± 4.4	1890 ± 60	19.8 ± 4.4
1408−078	166.2 ± 0.4	66.2 ± 3.2	24.9 ± 1.9	4526 ± 52	37.6 ± 1.9
1504+105	155.9 ± 0.4	105.0 ± 1.8	72.9 ± 0.7	3730 ± 29	83.3 ± 0.7
1512−090	117.4 ± 0.7	112.1 ± 1.5	114.6 ± 0.7	80 ± 26	114.8 ± 0.7
1513−100	157.5 ± 1.5	154.2 ± 1.9	154.6 ± 1.9	52 ± 38	154.8 ± 1.9
1540+147	154.8 ± 0.4	142.5 ± 0.6	140.5 ± 0.3	200 ± 11	141.1 ± 0.3
1550+054	144.9 ± 0.3	141.3 ± 0.5	139.8 ± 0.3	60 ± 9	140.0 ± 0.3
1608+104	161.7 ± 0.6	74.9 ± 2.6	65.7 ± 2.2	1399 ± 43	69.6 ± 2.2
1657+479	71.5 ± 0.7	148.5 ± 1.3	135.4 ± 8.4	1661 ± 23	140.0 ± 8.4
1800+784	111.7 ± 0.4	99.9 ± 0.8	97.2 ± 0.4	192 ± 14	97.8 ± 0.4
1801+440	49.9 ± 0.2	44.2 ± 0.5	48.5 ± 2.6	91 ± 9	48.8 ± 2.6
1824+568	33.2 ± 0.3	19.4 ± 1.1	15.4 ± 0.4	227 ± 18	16.1 ± 0.4
1849+670	143.9 ± 0.4	116.5 ± 3.6	155.4 ± 0.9	−5359 ± 57	140.4 ± 0.9
1902+318	44.2 ± 0.2	27.9 ± 2.4	43.2 ± 2.0	−2633 ± 39	35.9 ± 2.0
1939−154	157.0 ± 0.5	61.6 ± 5.9	29.8 ± 3.1	4437 ± 94	42.2 ± 3.1
2011−157	149.7 ± 0.9	124.6 ± 3.1	95.0 ± 8.3	3309 ± 52	104.3 ± 8.3
2143+176	142.4 ± 0.8	11.4 ± 1.7	13.7 ± 2.0	−786 ± 30	11.5 ± 2.0
2346+094	130.5 ± 0.2	150.3 ± 1.7	154.0 ± 1.5	−322 ± 27	153.1 ± 1.5
2358−102	122.8 ± 0.3	32.0 ± 5.5	17.1 ± 3.6	1470 ± 88	21.2 ± 3.6

Galactic contribution could be an explanation. Alternatively we note that a 5° systematic error in the position angle difference $\phi_{8.4} - \phi_{22}$, for example arising from mis-calibration, would correspond to an error in the estimated rotation measure of ±80 rad m^{-2} and hence such a systematic shift in the position angles could reduce, but not completely remove, the anomaly.

3 STATISTICAL PROPERTIES OF ALL DETECTED SOURCES INCLUDING INFORMATION FROM OTHER SURVEYS

In this section, we will use all the measurements we have made (including non-detections) plus information from the NVSS (Condon et al. 1997) at 1.4 GHz, additional information at 8.4 GHz from CLASS (Jackson et al. 2007) and measurements made at 86 GHz using the IRAM telescope (Agudo et al. 2009). In total, we have 191, 154, 169, 167 and 71 significant detections of polarization at the five frequencies. Before continuing, we note that the inclusion of this extra information could possibly lead to some extra scatter in the properties of the sources for two reasons. First the observations were not taken at the same time as our own and therefore they could be affected by source variability. In addition, the measurements were made at different resolutions. For example, those made by CLASS used a different array configuration (VLA A-configuration as opposed to D-configuration) which has 35 times higher resolution. This could lead to polarized emission being resolved out for sources with extended emission. This was pointed out by Jackson et al. (2010); in addition to the comments made there, we point out

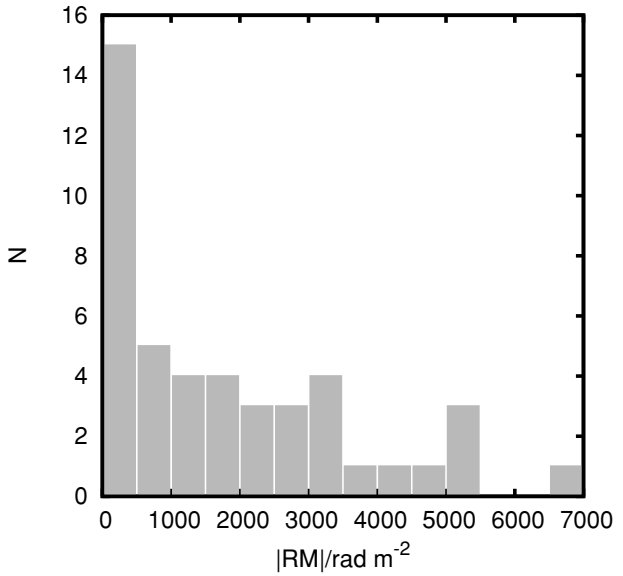

Figure 5. Histogram of the estimated modulus of the rotation measures for the 45 sources listed in Table 3. Note that there are a significant number of sources with $|\mathrm{RM}| > 1000\,\mathrm{rad\,m^{-2}}$.

that the average polarization of the 31 (out of 154) sources for which we are using a CLASS measurement, the average polarization percentage $100\langle\Pi\rangle \approx 2$ where it is $\approx$3 for the whole sample. In addition to extra scatter, we draw attention to the fact that the sample is now much more heterogeneous and this could affect the interpretation of the results. For example, we caution against making strong conclusions from the 86 GHz data which is just an incomplete sub-sample with lower signal-to-noise ratio than the other observations.

The statistical properties of the fractional polarization at the five frequencies are tabulated in Table 4. The values $\langle\Pi\rangle$ and $\langle\Pi^2\rangle^{1/2}$ (which are computed only from the detections) at 8.4, 22 and 43 GHz are similar to those found for the contemporaneous sample – although the values for 8.4 GHz are slightly lower due to the inclusion of the CLASS sources. In addition, we have also performed a survival analysis using the ASURV package (Lavalley, Isobe & Feigelson 1992) which attempts to take into account the upper limits on the fractional polarization when computing the statistical properties. We find that the estimates for $\langle\Pi\rangle$ and $\langle\Pi^2\rangle$ are in agreement with those obtained from detections only. We have also included the median fractional polarization, Π_{med}, taking into account the non-detections. This will be a more accurate representation of the true distribution than $\langle\Pi\rangle$ and we will use this in Section 6 to normalize the probability distribution for Π. The numbers are again compatible with there being no evolution in the properties between 8.4 and 43 GHz. The situation is different at 1.4 and 86 GHz. We see that $\langle\Pi\rangle$, $\langle\Pi^2\rangle^{1/2}$ and Π_{med} are significantly lower at 1.4 GHz and are higher at 86 GHz. These results are illustrated in the left-hand panel of Fig. 6 where we plot the distribution of Π as a function of frequency for those frequencies where the number of sources is approximately equal, that is 1.4–43 GHz. The histograms at 22 and 43 GHz are similar to those for the contemporaneous sample while that at 8.4 GHz is slightly modified by the inclusion of the CLASS sources. The histogram at 1.4 GHz is very different from the others. The overall distribution is shifted to lower values of Π and there is a long tail to lower values. This in not unexpected as it has been long known that the Faraday depolarization becomes an important factor at frequencies around 1.4 GHz (e.g. Garrington et al. 1988).

The range of values of total intensity for our sample is relatively low, making it difficult for us to investigate the variation of statistical properties with total intensity – this would require a comparison sample of data which was complete to a lower flux density limit, say to $\sim$100 mJy. None the less, we have attempted to investigate this issue. In the right-hand panel of Fig. 6, we present histograms of sub-samples split into two almost equal parts either side of 1.4 Jy. The two distributions appear to be almost identical, suggesting that, within this sample for which the total intensity is in the range $\approx$0.5 to $\approx$4.5 Jy, there is no evidence for evolution. Gawroński et al. (2010) point out that a variation of average polarization properties with flux density might be expected because the proportion of steep spectrum sources increases as the flux density limit is decreased. They compared the spectral index distributions of sources selected at 15 and 22 GHz over a wide range of total intensity flux density. We would expect that some evolution in the fractional polarization distribution will eventually emerge as sources with lower flux densities are studied and samples become increasingly dominated by steep spectrum extended sources.

Previous analyses of the polarization properties of sources in samples selected at lower frequencies than ours have suggested that steep spectrum sources typically have larger values of Π than compact flat spectrum sources (e.g. Gardner & Whiteoak, 1969). This is likely to be related to the high level of magnetic order in the synchrotron producing regions in extended regions of steep spectrum sources. We have attempted to search for any evidence for this in our sample. In the left-hand panel of Fig. 7 we have plotted the fractional polarization at 22 GHz, Π_{22}, against the spectral index between 1.4 and 43 GHz, $\alpha^{43}_{1.4}$. We have chosen this specific range in order for it to be optimal in separating steep and flat spectrum sources. We see that the vast majority of sources in the sample (130 out of 169) are flat spectrum ($|\alpha^{43}_{1.4}| < 0.3$), making it difficult to see the expected correlation between Π_{22} and $\alpha^{43}_{1.4}$. We have also plotted histograms of Π_{22} for the flat and steep spectrum sources,

Table 4. Statistical information for the fractional polarizations of the whole sample at the different frequencies. Those made using the survival analysis tool ASURV are also presented for 8.4–43 GHz. N_{det} is the number of detections at that frequency. At 8.4 GHz, there are 123 detections from the present observations and 31 taken from the CLASS sample which used the VLA at a different resolution (A-configuration as opposed to D-configuration). All detections at 1.4 GHz are taken from NVSS and those at 86 GHz from Agudo et al. (2009).

ν/GHz	N_{det}	$100\langle\Pi\rangle$	$100\langle\Pi^2\rangle^{1/2}$	$100\Pi_{\mathrm{med}}$	$100\langle\Pi\rangle_{\mathrm{ASURV}}$	$100\langle\Pi^2\rangle^{1/2}{}_{\mathrm{ASURV}}$
1.4	191	2.2	3.9	1.6		
8.4	154	2.9	3.5	2.5	2.9 ± 0.2	3.6 ± 0.9
22	169	3.1	3.9	2.0	3.0 ± 0.2	3.8 ± 1.0
43	167	3.5	4.3	2.3	3.5 ± 0.2	4.3 ± 1.3
86	71	4.5	5.1	4.0		

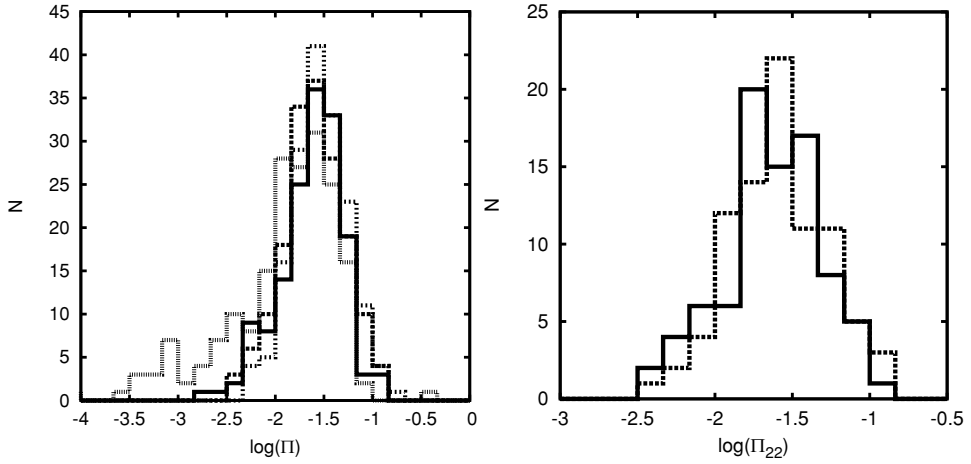

Figure 6. Left: histogram of the number of sources as a function of the logarithm of the fractional polarization, $\log_{10}(\Pi)$, for all detections including those detected at 8.4 GHz by CLASS only and at 1.4 GHz by NVSS. The fine dotted line is for 1.4 GHz, the solid line for 8.4 GHz, the dashed line for 22 GHz and the dotted line for 43 GHz. On the right is a split of the detections at 22 GHz into those with $S > 1.4$ Jy (solid line) and <1.4 Jy (dashed line).

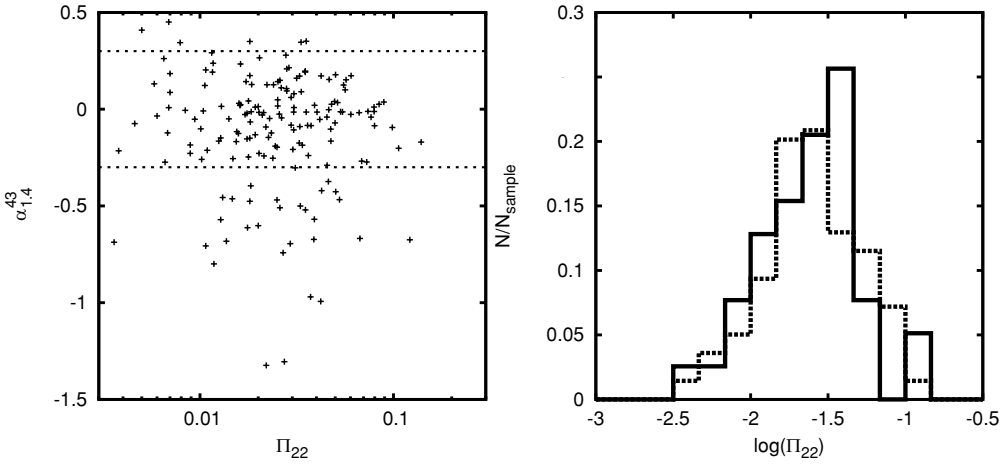

Figure 7. Left: scatter plot of the fractional polarization at 22 GHz (Π_{22}) against the intensity spectral index from 1.4 to 43 GHz ($\alpha^{43}_{1.4}$). The two horizontal lines enclose the flat spectrum region $|\alpha^{43}_{1.4}| < 0.3$. On the right is a histogram of the number of sources (divided by the number of sources in the sample) as a function of fractional polarization at 22 GHz (Π_{22}) for two samples. The dashed line is the flat spectrum sample with $|\alpha^{43}_{1.4}| < 0.3$ and the solid line is the steep spectrum sample with $|\alpha^{43}_{1.4}| > 0.3$. There appears to be no strong correlation between Π_{22} and $\alpha^{43}_{1.4}$, and the histograms for the two samples are almost identical.

normalized by the numbers of sources in each of the samples. The number of sources in the steep spectrum group is much lower and hence the random errors on their histogram are larger. Given this, it seems reasonable to conclude that there is no evidence for any difference in the properties of the two samples from our data.

We have made a preliminary investigation of the correspondence between our measurements at 22 and 43 GHz with those made at 86 GHz presented in Agudo et al. (2009). In Fig. 8, we present correlations between the properties of the sources at 43 and 86 GHz. We see that there are strong correlations between the total intensity, polarized intensity and fractional polarization at the two frequencies indicating, reassuringly, that the observations made with different telescopes, frequencies and resolutions and, probably most importantly, different times are related. Typically the intensity at 86 GHz is lower than that at 43 GHz as would be expected for a spectrum which is turning over, although there are a few sources for which the 86 GHz flux density is larger than that at 43 GHz. The polarized intensities at the two frequencies are comparable, albeit with a large dispersion, and therefore the typical fractional polarization is higher at 86 GHz. In addition, we see that for more than half of the sources the polarization position angles are within 20° indicating that those measured at 43 GHz (and 86 GHz) are close to the intrinsic position angle. We are, however, surprised by the tail of very large position angle differences. This tail is more evident than in the similar histogram for the difference in 22 and 43 GHz polarization position angles shown in fig. 6 of Jackson et al. (2010) thus arguing against Faraday rotation as being the explanation. We will return to this question below.

In Fig. 9, we present two-colour diagrams for the spectral indices between 22-43-86 GHz for total and polarized intensity, and a histogram for the intensity spectral index between 43 and 86 GHz. The two-colour diagram for polarized intensity is very similar to that between 8.4-22-43 GHz, whereas that for total intensity is very different. For 8.4-22-43 GHz, there is a strong correlation between $\alpha^{22}_{8.4}$ and α^{43}_{22} whereas no such correlation exists between α^{43}_{22} and α^{86}_{43}. We see that the range of values for α^{86}_{43} in the histogram is much

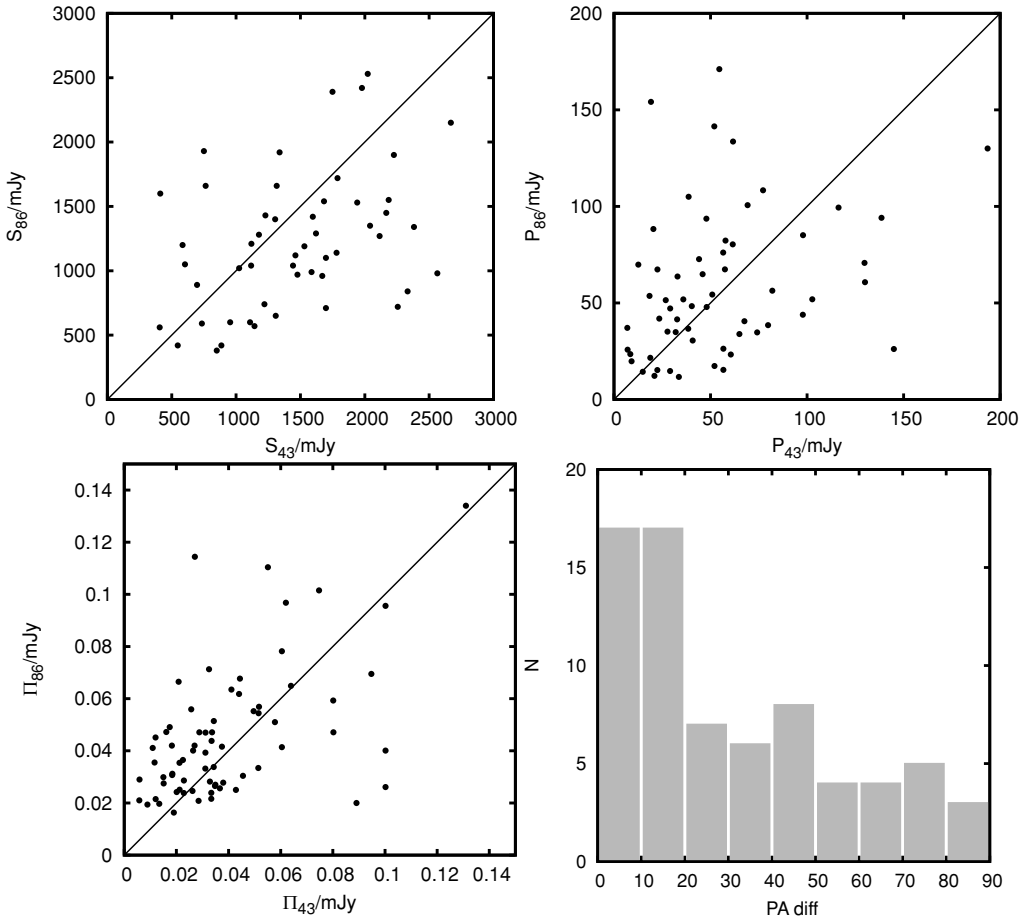

Figure 8. A comparison between the properties of sources measured at 43 and 86 GHz: (top left) total intensity; (top right) polarized intensity; (bottom left) fractional polarization; (bottom right) histogram of the difference in the polarization position angle. There are clear correlations between the measured properties at the two frequencies.

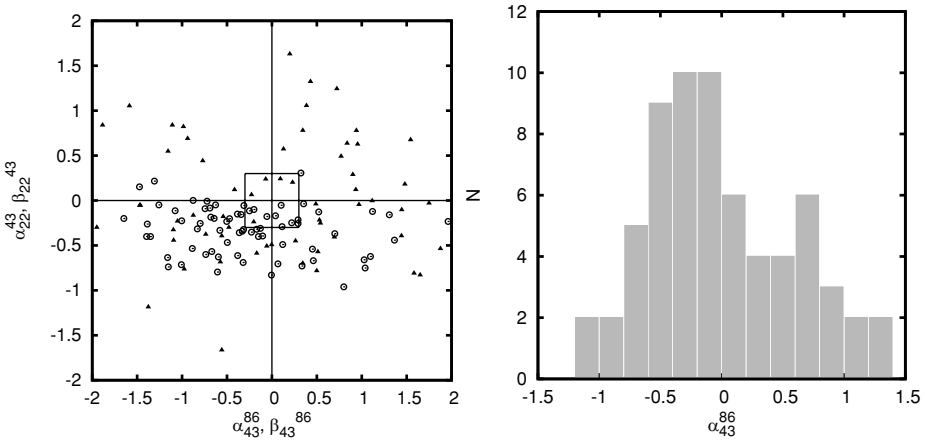

Figure 9. Left: the two-colour diagram for total (circles) and polarized (triangles) intensity for 22-43-86 GHz. For total intensity this is very different to that presented in Fig. 3 for 8.4-22-43 GHz. There is no obvious correlation between the two spectral indices. The two-colour diagram for polarized intensity is very similar to that for 8.4-22-43 GHz. On the right is a histogram of the total intensity spectral index between 43 and 86 GHz. The range of spectral indices presented here is substantially wider than seen between 22 and 43 GHz.

larger than that for α_{22}^{43} with a reasonable fraction of sources having $\alpha_{43}^{86} > 0$ indicating that the spectrum is rising when it was falling off between 22 and 43 GHz. This behaviour is unexpected and is difficult to explain without appealing to the effects of variability created by the non-contemporaneous observations.

4 DISCUSSION

The results presented in the earlier sections suggest a number of quantitative conclusions. The fractional polarization distribution is relatively independent of the frequency at which it is measured. We

have also seen no evidence for any dependence on total intensity flux density over the narrow range we have probed. In the subsequent analyses, we will assume that the median fractional polarization is completely independent of frequency and adopt the value $100\Pi_{\rm med} \approx 2.25$. There is some dependence of the rms fractional polarization for detected objects on the frequency of observation. If we assume that this dependence is linear then $100\langle\Pi^2\rangle^{1/2} = 3.310 + 0.023(\nu/{\rm GHz})$ which fits the data in the range $\nu = 8.4$ to 43 GHz. We note that while the quoted values for the median take into account the undetected sources, the computation of the rms uses only those which are detected, and hence it could be biased to larger values. We believe that this selection effect is mainly responsible for the observed frequency dependence of the rms fractional polarization since the general trend is for polarized intensity to be weaker at higher frequencies and hence fewer sources will actually be detected.

There is evidence for interesting behaviour revealed in the two-colour diagrams for total intensity, polarized intensity and fractional polarization. As expected, there is a strong correlation between the total intensity spectral indices; they satisfy the relation $-0.81\alpha^{22}_{8.4} + 0.58\alpha^{43}_{22} = -0.12 \pm 0.17$. The polarized intensity two-colour diagram is very different with apparently little correlation between $\beta^{22}_{8.4}$ and β^{43}_{22}. The combination of the strong correlation between total intensity spectral indices and no correlation between the polarization spectral indices leads to an anti-correlation between the fractional polarization spectral indices. One symptom of this is that there is fraction (∼25 per cent) of sources whose polarized intensity spectra are upturning between 8.4 and 43 GHz, in marked contrast to the case of total intensity for which there are no upturn sources.

The lack of correlation between the polarization spectral indices indicates that the polarized intensity spectra are less smooth than the total intensity spectra, that is, there are significant undulations in the polarized intensity spectra. Most of the sources in our sample have relatively flat total intensity spectra between 8.4 and 43 GHz due to their selection at 22 GHz. The standard explanation for this (Cotton et al. 1981) is that the sources' intensity spectra are made up of a number of synchrotron components whose net effect adds up to something which is close to a flat spectrum. This is illustrated in the left-hand panel of Fig. 10 . The fractional polarizations and polarization position angles of these components can vary with frequency for a variety of physical reasons, e.g. changes in the magnetic field direction, the degree of ordering of the field, spatially varying Faraday rotation and whether the components are optically thin or thick at the frequency of observation. All these effects can contribute to polarization spectra being more 'bumpy' than total intensity spectra. We have illustrated this in the right-hand panel of Fig. 10 where we have assumed, for example, that two of the components are 20 per cent polarized and the others 2 per cent polarized. This extra degree of freedom will make the polarization spectra less flat than their total intensity counterparts. The specific make up of the components and their distribution of fractional polarization could lead to the range of spectral type which we observe. In addition, the low-frequency spectrum of each of the component could be cut-off sharply by synchrotron self-absorption. Optically thick synchrotron emission is expected to be less polarized than optically thin emission (Ginzburg & Syrovatskii 1969).

It would be useful for the purpose of modelling the statistical properties of the polarized source population if there was a dependence of polarized flux upon total intensity spectral index. Such a dependence might be expected since optically thin, steep spectrum, sources generally have higher degrees of polarization at low frequencies and, therefore, the absence of a detectable correlation between the total intensity spectral index and the fractional polarization in our data might be thought surprising. However, we suspect that there are just too few steep spectrum sources in our sample of the strongest sources in the sky to see such an effect. It may become more evident when weaker samples in which the proportion of steep spectrum sources is higher (e.g. Gawroński et al. 2010) are studied.

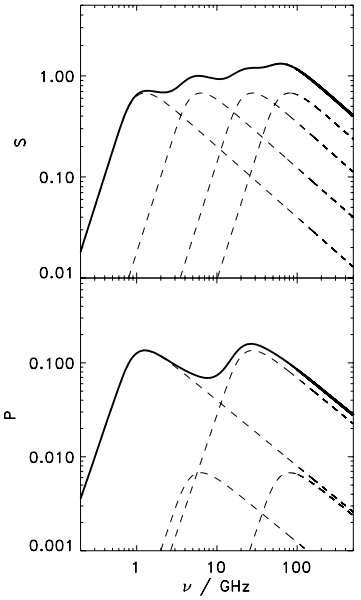

Figure 10. A schematic of the total (top) and polarized (bottom) intensity spectra of a flat-spectrum source in arbitrary units which is made up of four components which have different fractional polarizations – two with 20 per cent polarization and the other two with 2 per cent. In this example, the polarized intensity spectrum has two well-defined peaks, one around 1 GHz and the other between 20 and 30 GHz. From the point of view of our observations, this source would have a flat spectrum in total intensity and a peaked spectrum in polarized intensity. One could have easily created an example with an upturning spectrum in the range 8.4 to 43 GHz by exchanging the polarization fractions.

5 NOISE BACKGROUND FOR CMB POLARIZATION OBSERVATIONS

It is well understood that an ensemble of Poisson distributed point sources gives rise to a flat power spectrum in intensity (e.g. Cleary et al. 2005 and references therein). For sources below some cut-off $S_{\rm cut}$, the amplitude of this white noise spectrum is given by

$$C_\ell^{TT} = \left(\frac{{\rm d}B}{{\rm d}T}\right)^{-2}\langle S^2\rangle = \left(\frac{{\rm d}B}{{\rm d}T}\right)^{-2}\int_0^{S_{\rm cut}} {\rm d}S\, S^2\frac{{\rm d}N}{{\rm d}S}, \qquad (2)$$

where ${\rm d}N/{\rm d}S$ is the differential source count, ${\rm d}B/{\rm d}T = 2.5 \times 10^7 {\rm Jy\,sr^{-1}\,K^{-1}}\, x^4 e^x/(e^x-1)^2$ and $x = \nu/56.8\,{\rm GHz}$.

One could define an equivalent expression for the polarization spectrum

$$C_\ell^P = C_\ell^{\rm EE} + C_\ell^{\rm BB} = \left(\frac{{\rm d}B}{{\rm d}T}\right)^{-2}(\langle Q^2\rangle + \langle U^2\rangle)$$
$$= \left(\frac{{\rm d}B}{{\rm d}T}\right)^{-2}\int_0^{P_{\rm cut}} {\rm d}P\, P^2\frac{{\rm d}N}{{\rm d}P} \qquad (3)$$

in terms of the polarized source count ${\rm d}N/{\rm d}P$ and a cut-off in polarized intensity $P_{\rm cut}$. In what follows we will assume that the emission will, on average, contribute equally to the EE and BB power spectra, that is $C_\ell^{\rm EE} = C_\ell^{\rm BB} = \frac{1}{2}C_\ell^{\rm P}$. However, the polarized

source counts are difficult to measure since the polarized signal is weak and most samples are defined by their completeness in terms of total intensity. It has been suggested (de Zotti et al. 1999; Mesa et al. 2002; Tucci et al. 2004) that one should use the intensity source count supplemented by information on the statistical properties of Π defined by some probability density function $\mathcal{P}(\Pi)$ which for the purposes of our discussion we will assume is independent of the total intensity of the source. This is supported by our observations for a narrow range of flux densities $\sim$1 Jy, but may not be true for lower values.

One approach (method A) is to define the noise spectrum in terms of a cut-off in total intensity, $S_{\rm cut}$. This is likely to be most useful in practice since one could imagine having a high-resolution survey complete to some level in total intensity, as opposed to the equivalent in polarized intensity. In this case, one can define the power spectrum due to sources with a given fractional polarization, Π, as

$$C_\ell^P(\Pi) = \left(\frac{{\rm d}B}{{\rm d}T}\right)^{-2}\int_0^{\Pi S_{\rm cut}} {\rm d}P\, P^2 \frac{{\rm d}N}{{\rm d}P} = \left(\frac{{\rm d}B}{{\rm d}T}\right)^{-2}\Pi^2\int_0^{S_{\rm cut}} {\rm d}S\, S^2\frac{{\rm d}N}{{\rm d}S}. \tag{4}$$

The spectrum due to all the sources is then given by

$$C_\ell^P = \int_0^1 {\rm d}\Pi\, \mathcal{P}(\Pi) C_\ell^P(\Pi) = \langle\Pi^2\rangle C_\ell^T, \tag{5}$$

where $\langle\Pi^2\rangle = \int_0^1 {\rm d}\Pi\, \Pi^2\mathcal{P}(\Pi)$.

Another approach (method B) is to attempt to compute the noise spectrum due to sources in terms of a cut-off in polarized intensity, $P_{\rm cut}$. If we define the spectrum due to sources with fractional polarization Π to be

$$C_\ell^P(\Pi) = \left(\frac{{\rm d}B}{{\rm d}T}\right)^{-2}\int_0^{P_{\rm cut}} {\rm d}P\, P^2 \frac{{\rm d}N}{{\rm d}P} = \left(\frac{{\rm d}B}{{\rm d}T}\right)^{-2}\Pi^2\int_0^{P_{\rm cut}/\Pi} {\rm d}S S^2\frac{{\rm d}N}{{\rm d}S}, \tag{6}$$

the spectrum due to all sources is then given by

$$\begin{aligned} C_\ell^P &= \int_0^1 {\rm d}\Pi \mathcal{P}(\Pi) C_\ell^P(\Pi) \\ &= \left(\frac{{\rm d}B}{{\rm d}T}\right)^{-2}\int_0^1 {\rm d}\Pi\Pi^2\mathcal{P}(\Pi)\int_0^{P_{\rm cut}/\Pi} {\rm d}S\, S^2\frac{{\rm d}N}{{\rm d}S}, \end{aligned} \tag{7}$$

which can be rewritten as

$$C_\ell^P = \left(\frac{{\rm d}B}{{\rm d}T}\right)^{-2}\left[\langle\Pi^2\rangle\int_0^{P_{\rm cut}} {\rm d}S S^2\frac{{\rm d}N}{{\rm d}S} + \int_{P_{\rm cut}}^\infty {\rm d}S S^2\frac{{\rm d}N}{{\rm d}S} F\left(\frac{P_{\rm cut}}{S}\right)\right], \tag{8}$$

where the weighting function

$$F(x) = \int_0^x \Pi^2\mathcal{P}(\Pi)\,{\rm d}\Pi, \tag{9}$$

and we have that $F(1) = \langle\Pi^2\rangle$.

In order to estimate the error involved in using method A compared to method B, one can compute the ratio of the two noise power spectra (method B over method A) for $P_{\rm cut} = \langle\Pi\rangle S_{\rm cut}$. This is given by

$$R = \frac{\int_0^\infty {\rm d}S\, S^2\frac{{\rm d}N}{{\rm d}S} G\left(\frac{\langle\Pi\rangle S_{\rm cut}}{S}\right)}{\int_0^{S_{\rm cut}} {\rm d}S\, S^2\frac{{\rm d}N}{{\rm d}S}}, \tag{10}$$

where $G(x) = F(x)/F(1)$ for $x < 1$ and $G(x) = 1$ for $x > 1$.

In view of the observed distributions of the fractional polarization (see Fig. 1), it should be possible to model $\mathcal{P}(\Pi)$ using a Gaussian in $\log\Pi$, that is

$$\mathcal{P}(\Pi) = \frac{A}{\Pi}\exp\left[-\frac{\left[\log\left(\frac{\Pi}{\Pi_0}\right)\right]^2}{2\sigma^2}\right], \tag{11}$$

in the range $0 \le \Pi \le 1$. For a standard lognormal distribution, for which $0 \le \Pi < \infty$, the normalization coefficient, A, can be computed to be $(2\pi\sigma^2)^{-1/2}$, Π_0 is the median and σ is the standard deviation in log. Due to the fact that the upper limit of the distribution is $\Pi = 1$, these need to be adjusted. For the particular choices of Π_0 and σ which we will choose, $\Pi = 1$ will be sufficiently large so as to be effectively infinite and these adjustments will be sub-dominant, but we have included them below for completeness.

For this particular choice of probability density function, one finds that

$$\begin{aligned} A &= \sqrt{\frac{1}{2\pi\sigma^2}}\left[\frac{2}{1+{\rm erf}\left(\frac{\log(1/\Pi_0)}{\sqrt{2}\sigma}\right)}\right], \\ \langle\Pi\rangle &= \Pi_0 e^{\frac{1}{2}\sigma^2}\left[\frac{1+{\rm erf}\left(\frac{\log(1/\Pi_0)}{\sqrt{2}\sigma}+\frac{1}{\sqrt{2}}\sigma\right)}{1+{\rm erf}\left(\frac{\log(1/\Pi_0)}{\sqrt{2}\sigma}\right)}\right], \\ \langle\Pi^2\rangle &= \Pi_0^2 e^{2\sigma^2}\left[\frac{1+{\rm erf}\left(\frac{\log(1/\Pi_0)}{\sqrt{2}\sigma}+\sqrt{2}\sigma\right)}{1+{\rm erf}\left(\frac{\log(1/\Pi_0)}{\sqrt{2}\sigma}\right)}\right], \end{aligned} \tag{12}$$

$$\Pi_{\rm med} = \Pi_0\exp\left[\sqrt{2}\sigma\,{\rm erf}^{-1}\left[\frac{1}{2}\left({\rm erf}\left(\frac{\log(1/\Pi_0)}{\sqrt{2}\sigma}\right)-1\right)\right]\right], \tag{13}$$

where the terms inside the square brackets in the first three expressions are the corrections which would $\to 1$ if $\log(1/\Pi_0) \to \infty$ and the argument for the exponential will $\to 0$ in the same limit. One can also compute the weighting function

$$F(x) = \Pi_0^2 e^{2\sigma^2}\left[\frac{1+{\rm erf}\left(\frac{\log(x/\Pi_0)}{\sqrt{2}\sigma}+\sqrt{2}\sigma\right)}{1+{\rm erf}\left(\frac{\log(1/\Pi_0)}{\sqrt{2}\sigma}\right)}\right]. \tag{14}$$

6 PREDICTIONS FOR THE NOISE BACKGROUND

In order to make predictions of the contamination of CMB polarization observations from point sources we need to have a model for the differential source count $n(S) = {\rm d}N/{\rm d}S$ as a function of frequency. We have used the dZ05 model (de Zotti et al. 2005) which is available at a range of suitable frequencies.[1] We have adopted the lognormal probability distribution (12) with $100\Pi_0 = 2.25$ and $\sigma = 0.74$, independent of frequency, which gives $100\langle\Pi\rangle = 2.9$ and $100\langle\Pi^2\rangle^{1/2} = 3.9$ compatible with the observed values at 22 GHz. The differential source counts at 30 GHz and 150 GHz, along with measured source counts from Wright et al. (2009), Cleary et al. (2005) and Gawroński et al. (2010) at 30 GHz and Viera et al. (2010) and Marriage et al. (2010) at $\sim$150GHz, and the probability distributions are presented in Fig. 11. We also included predicted source counts at 30 GHz from Toffolatti et al. (1998, hereafter T98) for comparison. The values of Π_0 and σ were chosen to give the measured values for the median and the rms $\langle\Pi^2\rangle^{1/2}$. We also include a curve using $100\Pi_0 = 2.5$ and $\sigma = 0.67$, values which are

[1] See http://web.oapd.inaf.it/rstools/srccnt/srccnt_tables.html

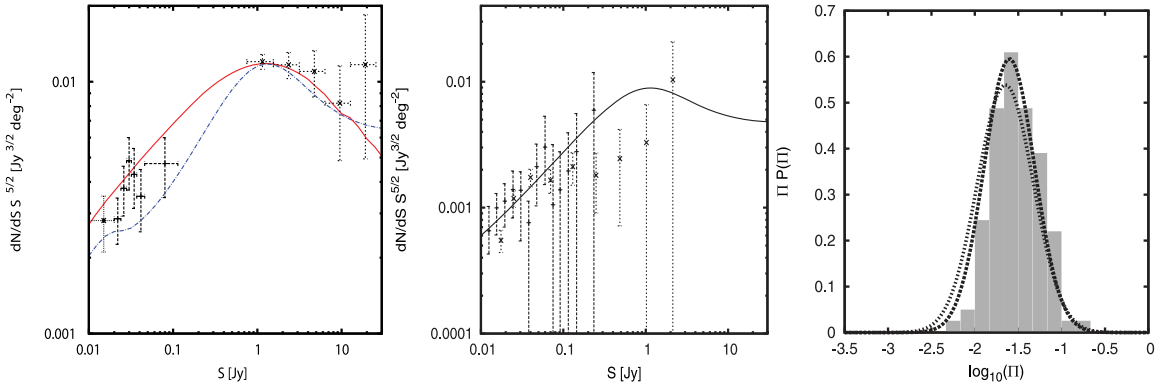

Figure 11. Left: the source surface density at 30 GHz against flux density from the dZ05 model (blue) and the T98 model (red). Note that they agree in the region of 1 Jy but differ significantly at lower flux densities. Included also are measured source counts from Wright et al. (2009), Cleary et al. (2005) and Gawroński et al. (2010). Middle: the source surface density at 150 GHz for the dZ05 model. Included also are the measured source counts from Vieira et al. (2010) and Marriage et al. (2010). Right: the probability distribution (for logarithmic bins) for the fractional polarization with $100\Pi_0 = 2.25$, $\sigma = 0.74$ (dotted line) and $100\Pi_0 = 2.5$, $\sigma = 0.67$ (dashed line) along with the histogram for detected sources at 22 GHz.

chosen to give the measured values of $\langle\Pi\rangle$ and $\langle\Pi^2\rangle^{1/2}$ for the contemporaneously detected sample at 22 GHz. Note that this second set of values agrees well with the histogram of *detected* sources, but the values we have chosen for the subsequent analysis are more realistic since they taken into account undetected sources.

We have presented the results using method A in the left-hand panel of Fig. 12 as a function of $S_{\rm cut}$ for a range of frequencies popular for CMB observations. We plot $C_\ell^{\rm BB} = C_\ell^P/2$ and have included lines which represent the expected power spectrum amplitude for $r = 0.1$, 0.01 and 0.001 at the maximum of the B-mode power spectrum ($\ell \approx 80$). This is indicative of the level of foreground source subtraction required so as not to inhibit the detection of a gravitational wave induced B-mode polarization signal. It has been chosen as reference point, not as the precisely calculated requirement, since this would depend on the resolution of the instrument. As expected the point source noise level increases with $S_{\rm cut}$, asymptoting at higher values and is larger for lower frequencies.

We have computed the value of $C_\ell^{\rm BB}$ as a function of frequency for $S_{\rm cut} = 100, 1, 0.1, 0.01$ Jy. The cut-off of 100 Jy is effectively infinite as there are no sources with flux density greater than this. This is presented in the right-hand panel of Fig. 12 and illustrates the level of point source noise one would expect if no source subtraction is performed. It appears to show that it would be possible to detect $r = 0.1$ at frequencies greater than around 100 GHz without any subtraction. Some of the same information is presented in Fig. 13 which shows the power spectra from the point sources and those expected from the primordial CMB signal. This gives a more detailed picture of what level of source subtraction is required to achieve a detection at a given value of r as a function of resolution.

In order to assess the feasibility of source subtraction, it is important to know how many sources one might have to identify and extract from a map. In Fig. 14, we have computed the expected number of sources above $S_{\rm cut}$ for $\nu = 30$–220 GHz. The first thing to note is that this is relatively independent of ν; there is less than a factor of 2 between the prediction at 30 GHz and that at 220 GHz. This may seem a little paradoxical since we have seen that the effect of the sources on the power spectrum is strongly dependent on frequency. The reason for this is frequency dependence of the conversion factor between brightness temperature and flux density,

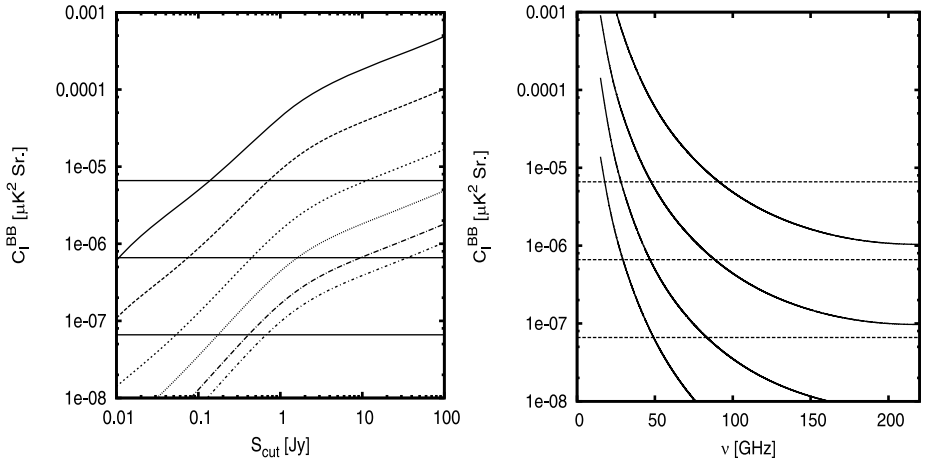

Figure 12. Left: the projected point source noise spectrum, $C_\ell^{\rm BB}$, as a function of $S_{\rm cut}$ for a range of frequencies (30 GHz – solid line, 44 GHz – dashed line, 70 GHz – coarse dotted line, 100 GHz – fine dotted line, 150 GHz – long–dashed dotted line, 220 GHz – short-dashed dotted line. The three horizontal lines correspond to the power spectrum amplitudes at the maximum ($\ell = 80$) of the B-mode spectrum for $r = 0.1$, 0.01 and 0.001 from top to bottom. Right: the point source noise spectrum for $S_{\rm cut} = 100$, 1, 0.1, 0.01 Jy (top to bottom) as a function of frequency. $S_{\rm cut} = 100$ Jy corresponds to the level of noise we predict for no source subtraction.

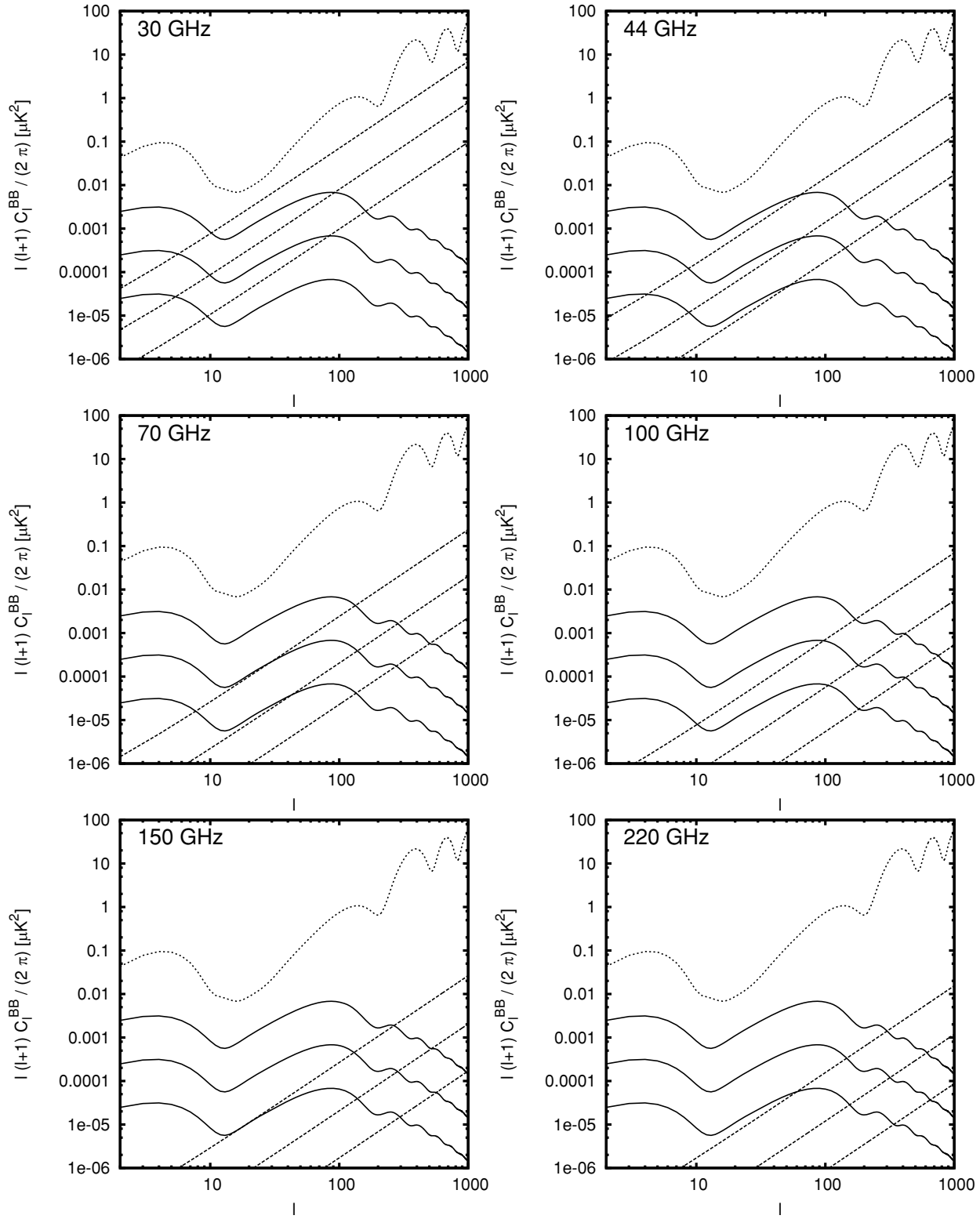

Figure 13. The projected noise spectra for a range of frequencies and $S_{\rm cut}$. On each plot there are spectra for three values of $S_{\rm cut} = 1$ Jy, 100 mJy and 10 mJy. Included also are a typical E-mode spectrum and B-mode spectra for $r = 0.1$, 0.01 and 0.001. The plots are for 30 GHz (top left), 44 GHz (top right), 70 GHz (middle left), 100 GHz (middle right), 150 GHz (bottom left) and 220 GHz (bottom right).

dB/dT: sources $\sim$1 Jy correspond to substantially higher thermodynamic brightness temperatures at low frequencies. For subtraction at the level of $S_{\rm cut} = 1$ Jy, where most of the sources are likely to have been already identified, there is $\approx$1 source per 200 deg^2 which would have to be removed. For $S_{\rm cut} = 100$ mJy for which a moderate-sized program would have to be mounted using, for example, a dedicated instrument or the VLA, there would be $\approx$1 source per 8 deg^2.

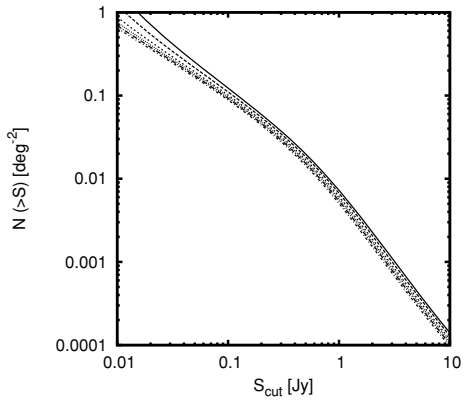

Figure 14. The number of sources per square degree which need to be removed from a map for a given value of $S_{\rm cut}$. Curves are included for each of the frequencies 30, 40, 70, 100, 150, 220 GHz used in the earlier plots using the same line convention as in Fig. 13. We note that they are all very similar.

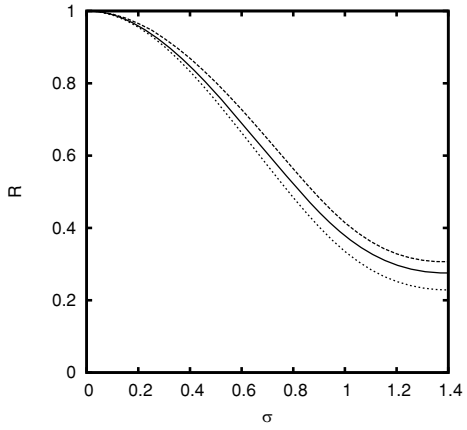

Figure 15. The ratio R of the noise spectrum from methods A and B as a function of the scatter σ for $\nu = 30$ GHz. The three different curves are for $S_{\rm cut} = 1$ Jy (solid line), 100 mJy (dashed line) and 10 mJy (dotted line).

We note that the estimate above only includes the effects of point sources which are dominated by synchrotron emission and hence can be identified at low frequencies. It is well known that CMB observations at higher frequencies (greater than $\sim$100 GHz) are contaminated by dust emission from star-forming galaxies at high redshift (Scott & White 1999). There is very little information available about the polarization of such objects but one would expect it to be relatively low since the alignment between the magnetic fields and dust grains in these objects is likely to be disordered, leading to low fractional polarization when integrated over the whole galaxy. The only information available at present for this population is for the local starburst galaxies Arp 220 for which there is an upper limit of $100\Pi < 1.5$ at 353 GHz (Seiffert et al. 2007) and M82 which has been estimated to have $100\Pi \approx 0.4$ at the same frequency (Greaves & Holland 2002).

In order to estimate the confusion noise from this component we have to not only include the contribution from Poisson fluctuations, but also that from the clustering of the sources. We have been able to make an estimate for the Poisson contribution by making the assumption that $100\langle\Pi^2\rangle^{1/2} = 1$ and have used the differential source count at 350 GHz suggested in Borys et al. (2003)

$$\frac{{\rm d}N}{{\rm d}S} = N_0/S_0 \left[\left(\frac{S}{S_0} \right)^{\alpha} + \left(\frac{S}{S_0} \right)^{\beta} \right]^{-1}, \quad (16)$$

where $S_0 = 1.8$ mJy, $\alpha = 1.0$, $\beta = 3.3$ and $N_0 = 1.5 \times 10^4$ deg^{-2}. The extrapolation to lower frequencies is made using $S \propto \nu^{\gamma}$ where $\gamma \approx 3.5$ compatible with the measurements of Hall et al. (2010). We find that $C_\ell^P = 9 \times 10^{-9}$ μK^2 sr at 150 GHz, 2×10^{-8} μK^2 sr at 220 GHz and 3×10^{-7} μK^2 sr at 350 GHz compatible with the values presented in Seiffert et al. (2007). It appears that Poissonian contribution of these dusty galaxies is sub-dominant to our estimate of the contribution from synchrotron-dominated sources in this frequency range, though one should note our earlier remark that the radio source contribution may be overestimated. Irrespective of this, it seems unlikely that the Poissonian contribution will have a significant impact on our ability to detect B-mode polarization for $r > 0.01$ below 220 GHz unless there is a significant population of sources with $100\Pi \gg 1$. However, the galaxies are expected to be significantly clustered. At present, the scale of this effect is somewhat uncertain, but most studies (e.g. Negrello et al. 2007) appear to find a significant contribution to the confusion noise in total intensity, and observations are starting to constrain its amplitude (see Hall et al. 2010). The exact impact of this effect will be better understood when the results from the *Planck* satellite become available, which will significantly increase our knowledge of this population of galaxies over a range of frequencies.

Finally, in Fig. 15 we have investigated the possible uncertainties in using method A by setting $P_{\rm cut} = \langle\Pi\rangle S_{\rm cut}$ in method B. We have computed the ratio R (the confusion noise from method B divided by that from method A) as a function of the scatter σ. For $\sigma = 0$ the two methods give the same answer, that is, $R = 1$ as expected, whereas for large values of σ we find that $R < 1$, that is, one finds that method A overpredicts the level of point source contamination when compared to model B. This might seem counterintuitive since one might expect a number of sources with unusually large fractional polarizations to scatter upwards. One can confirm this behaviour by computing R for a power-law differential source count ${\rm d}N/{\rm d}S \propto S^{-\alpha}$ for $\alpha < 3$. We find that $R \propto \exp[\sigma^2\alpha(\alpha - 3)/2]$ which decreases as σ increases.

7 COMPARISON WITH PLANK SKY MODEL

In order to make a comparison with previous work we have investigated the power spectrum of polarized extragalactic sources in the *Planck* Sky Model (PSM) version 1.6.6.[2] The radio source model is based on sources from low-frequency surveys extrapolated to higher frequencies with simple power laws for each source. The total intensity spectra are adjusted above 20 GHz to agree with *WMAP* measurements as well as remaining consistent with the source count model of de Zotti et al. (2005). Polarization properties are based on the polarization fraction distribution for a sample of sources observed with ATCA at 18.5 GHz (Ricci et al. 2004) and an assumption of random position angles. A summary of the complete source model is given in Massardi, Gonzales-Nuevo & de Zotti (2006).

In the left-hand panel of Fig. 16, we present the fractional polarization distribution for simulated sources extracted from the PSM with flux density greater than 1 Jy along with the model for $P(\Pi)$ we have used in Section 6. There appears to be good agreement with

[2] http://www.apc.univ-paris7.fr/APC_CS/Recherche/Adamis/PSM/psky-en.php

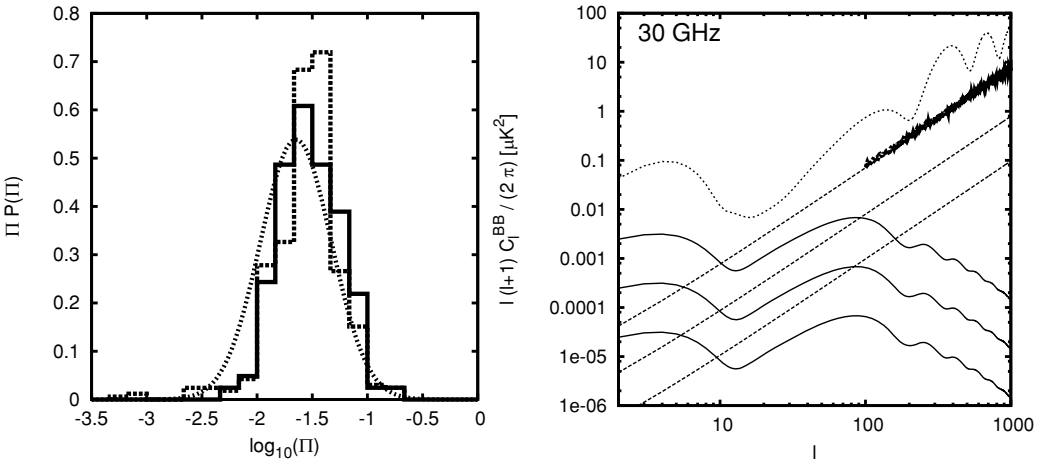

Figure 16. On the left is the fractional polarization distribution for source with flux density >1 Jy from the PSM compared to that from our sample selected at 22 GHz and the distribution we used in Section 6. On the right is the top-left-hand panel of Fig. 13 with the reconstructed power spectrum from the PSM at 30 GHz for sources less than 1 Jy included.

that found in our work implying that there are similarities between fractional polarization distribution of our sample and that of Ricci et al. (2004).

A full-sky realization of extragalactic sources was made at 30 GHz with a limiting flux cut-off of 1 Jy. The power spectrum was calculated using the PolSpice software v02-06-09[3] (Chon et al. 2004) for Galactic latitudes $>5^\circ$. Fig. 16 (right-hand panel) shows the reconstructed B-mode spectrum from the PSM simulation in the range $\ell = 100$–1000 for a flux cut-off of 1 Jy along with the predicted noise spectra from our model. The agreement with that presented in Fig. 13 is extremely good by virtue of the polarization fraction distribution being close to ours and the source count in the PSM, measured to be $S^{5/2}\mathrm{d}N/\mathrm{d}S \approx 0.012\,\mathrm{Jy}^{3/2}\,\mathrm{deg}^{-2}$, being very similar to the dZ05 model around 1 Jy. In the range of flux densities where our observations are relevant the two models appear to agree. We do not compare lower flux density cuts since the PSM is incomplete below ∼100 mJy.

8 SUMMARY AND CONCLUSIONS

We have presented some statistical properties of polarized radio sources from our observations of the *WMAP* point source catalogue at 8.4, 22 and 43 GHz. The main results are as follows.

(i) The median level of fractional polarization is around 2–2.5 per cent and there is no evidence for any dependence on frequency in the range 8.4 to 43 GHz.

(ii) We have argued that our data are compatible with the spectra in polarized intensity being less smooth than those in total intensity.

(iii) There is no evidence for a strong correlation between a single intensity spectral index and the fractional polarization, although most of our sources are flat spectrum.

(iv) We were able to compute rotation measures for 45 out of the 105 sources which were detected contemporaneously at all three frequencies.

(v) There is statistical evidence for large rotation measures with a significant number of sources having rotation measures $>1000\,\mathrm{rad\,m^{-2}}$.

We then used our results, in conjunction with the dZ05 model, to model the polarized source counts in order to compute the level of confusion noise expected in CMB polarization experiments designed to detect primordial gravitational waves from inflation. We find the following.

(i) The source confusion due to jet-powered radio sources is likely to be the dominant contribution to the total up to relatively high frequencies – in our estimates they even dominate at 220 GHz but we have also pointed out that this could be an artefact of our assumption of a single spectral index for each source.

(ii) Source subtraction will be important at frequencies below 100 GHz if one is to detect $r \sim 0.1$;

(iii) If one is to detect $r \sim 0.01$ some source mitigation strategy will be required at all frequencies.

In addition, there appears to be good agreement with our modelling and that in the PSM at 30 GHz for flux densities ≈1 Jy.

There is one final point we should make. Many of the sources, particularly those with high flux densities, are expected to be significantly variable. This will manifest itself not only in variable total and polarized flux densities, but also in the polarization position angle. This could make it difficult to subtract the effects of source confusion from the CMB polarization signal. If the observations of a particular CMB field are performed over a time-scale which is shorter than the time-scale of variability, this will require the high-resolution observations performed to assist source subtraction to take place contemporaneously in order to make an accurate subtraction. Conversely, if the time-scale for observations is longer than the variability, for example, if observations on a particular region are built up a series of short integrations over many days, then the variability of the source polarization could easily average out to a significantly lower observed polarization when the individual integrations are stacked. This effect will make accurate source subtraction difficult since it is likely to be impractical to monitor the level of variability for a substantial number of sources.

ACKNOWLEDGMENTS

The authors acknowledge the use of the PSM, developed by the Component Separation Working Group (WG2) of the *Planck* Collaboration. We thank G. de Zotti and M. Massardi for helpful

[3] http://www.planck.fr/article141.html

clarifications. CD acknowledges an STFC advanced fellowship and ERC grant under FP7.

REFERENCES

Agudo I., Thum C., Wiesemeyer H., Krichbaum T. P., 2009, ApJS, 189, 1
Baumann D. et al. [CMBPol Study Team Collaboration], 2009, AIP Conf. Proc., 1141, 10
Borys C., Chapman S. C., Halpern M., Scott D., 2003, MNRAS, 344, 385
Brown M. L. et al. [QUaD Collaboration], 2009, ApJ, 705, 978
Browne I. W. A. et al., 2003, MNRAS, 341, 13
Chiang H. C. et al., 2010, ApJ, 711, 1123
Chon G., Challinar A., Prunet S., Hiron E., Szapudi, 2004, MNRAS, 350, 914
Cleary K. A. et al., 2005, MNRAS, 360, 340
Condon J. J., Cotton W. D., Greisen E. W., Yin Q. F., Perley R. A., Taylor G. B., Broderick J. J., 1998, AJ, 115, 1693
Cotton W. D. et al., 1981, ApJ, 238, L123
de Zotti G., Gruppioni C., Ciliegi P., Burigana C., Danese L., 1999, New Astron., 4, 481
de Zotti G., Ricci R., Mesa D., Silva L., Mazzotta P., Toffolatti L., Gonzalez-Nuevo J., 2005, A&A, 431, 893
Gardner F. F., Whiteoak J. B., 1969, Australian J. Phys., 22, 107
Garrington S. T., Leahy J. P., Conway R. G., Laing R. A., 1988, Nat, 331, 147
Gawroński M. P. et al., 2010, MNRAS, 406, 1853
Ginzburg V. L., Sgrovatskii S. I., 1969, ARA&A, 7, 375
Greaves J. S., Holland W. S., 2002, AIP Conf. Proc., 609, 267
Hall N. R. et al., 2010, ApJ, 718, 632
Jackson N., Battye R. A., Browne I. W. A., Joshi S., Muxlow T. W. B., Wilkinson P. N., 2007, MNRAS, 376, 371
Jackson N., Browne I. W. A., Battye R. A., Gabudza D., Taylor A. C., 2010, MNRAS, 401, 1388
Kovac J., Leitch E. M., Pryke C., Carlstrom J. E., Halverson N. W., Holzapfel W. L., 2002, Nat, 420, 772
Lavalley M., Isobe T., Feigelson E., 1992, Astronomical Data Analysis Software and Systems I, 25, 245
Lopez-Caniego M., Massardi M., Gonzalez-Nuevo J., Lanz L., Herranz D., de Zotti G., Sanz J. L., Argueso F., 2009, ApJ, 705, 868
Marriage T. A. et al., 2010, preprint (arXiv:1010.1065)
Massardi M., Gonzales-Nuevo J., de Zotti G., 2006, 'Realistics Point Source Maps at Planck Frequencies. CMB and Physics of the Early Universe. Proceedings of Science, PoS p. 045
Massardi M. et al., 2008, MNRAS, 384, 773
Mesa D., Baccigalupi C., De Zotti G., Gregorini L., Mack K. H., Vigotti M., Klein U., 2002, A&A, 396, 463
Montroy T. E. et al., 2006, ApJ., 647, 813
Murphy T. et al., 2010, MNRAS, 402, 2403
Myers S. et al., 2003, MNRAS, 341, 1
Negrello M., Perrotta F., Gonzalez-Nuevo J., Silva L., de Zotti G., Granato G. L., Baccigalupi C., Danese L., 2007, MNRAS, 377, 1557
Page L. [WMAP Collaboration] et al., 2007, ApJS, 170, 335
Readhead A. C. S. et al., 2004, Sci, 306, 836
Ricci R. et al., 2004, A&A, 415, 549
Sadler E. M. et al., 2006, MNRAS, 371, 898
Scott D., White M. J., 1999, A&A, 346, 1
Seiffert M., Borys C., Scott D., Halpern M., 2007, MNRAS, 374, 409
Taylor A. R., Stil J., Sunstrum C., 2009, ApJ, 702, 1230
Toffolatti L., Argeso Gomez F., De Zotti G., Mazzei P., Franceschini A., Danese L., Burigana C., 1998, MNRAS, 297, 117 (T98)
Tucci M., Martinez-Gonzalez E., Vielva P., Delabrouille J., 2005, MNRAS, 360, 935
Vieira J. D. et al., 2010, ApJ, 719, 763
Zavala R. T., Taylor G. B., 2003, ApJ, 589, 126

APPENDIX A: CORRELATIONS BETWEEN OBSERVED QUANTITIES

In this Appendix, we present an analysis of the correlations between S_{ν_i} and P_{ν_i} for each of the three frequencies for the contemporaneous sample. In Fig. A1, we present a series of plots exhibiting the correlations between the six observed quantities. There are strong correlation (the correlation coefficient >0.5) between all six quantities with some, for example those between the intensity at the three frequencies having very high correlation coefficients (>0.7). These correlations lend support to our assumption that the sample of data contains considerable information and the polarization measurements are not dominated by noise.

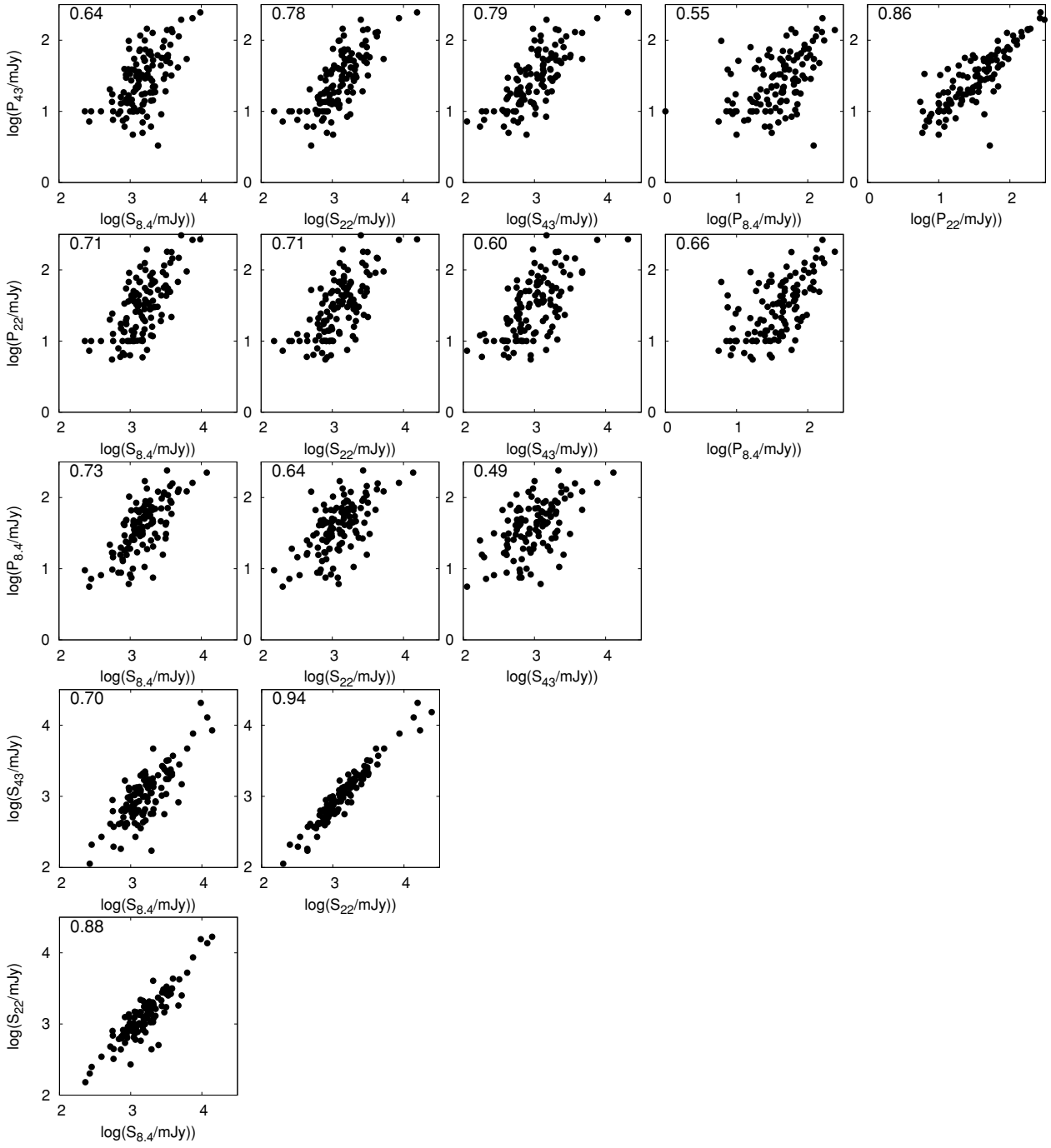

Figure A1. Correlations between the six observed quantities, the three intensities and the three polarized intensities, for the contemporaneous sample, along with a table of the correlation coefficients. It is clear that there are strong correlations between most of the quantities.

This paper has been typeset from a TEX/LATEX file prepared by the author.